Frequency Modulation Technique for MEMS Resistive Sensing

Ali Mohammadi, *Member, IEEE*, Mehmet Rasit Yuce, *Senior Member, IEEE*, and S. O. Reza Moheimani, *Fellow, IEEE*

***Abstract*— Frequency modulation technique can be applied to microelectromechanical systems (MEMS) transducers that require some form of resistive sensing. For example, electrothermal sensing is being investigated as a viable means of measuring displacement in micromachined transducers. This paper proposes a highly sensitive readout circuit, which can convert 10 Ω change of resistance in a 400 Ω electrothermal sensor to more than 200 kHz frequency variation (350–550 KHz). The frequency variations are then converted to voltage values by means of a frequency demodulation. In addition, the proposed technique achieves high linearity from the voltage applied to the actuator to the voltage measured at the sensor's output, which can potentially eliminate the need for an additional linearization if the sensor is used in a feedback loop. The proposed approach leads to high sensitivity in the MEMS electrothermal sensing since the method is not affected by amplitude variations that could arise from the readout circuit.**

***Index Terms*— Electrothermal sensing, frequency modulation, linearity, microelectromechancial systems.**

I. Introduction

THE DESIGN of (microelectromechanical system) MEMS transducers is a multi-disciplinary area of research that spans fields as diverse as circuit design and device physics in electronics to mechanics and thermodynamics. Two interesting applications of MEMS to emerge in recent years are nanopositioners and microgrippers. Nanopositioners have found applications in scanning probe microscopy [1], atomic force microscopy [2] and ultra-high-density probe storage system [3]. Microgrippers are utilized for manipulation of sub-micrometer-sized objects and biological cells [4], [5]. A typical device consists of high precision sensors and actuators plus a feedback control loop. The displacement produced by the actuator is measured by a sensor, whose output is fed back to the actuator to increase positioning accuracy of the system. As illustrated in Fig. 1, precise positioning is achieved through acquiring the location or displacement of the actuator by a sensor and its application via a feedback loop to the actuator input. Several sensing techniques for precise control of MEMS micro-actuators have been proposed, offering high sensing accuracy. For instance, in [6] piezoresistive sensor is used to measure the displacement of an actuator.

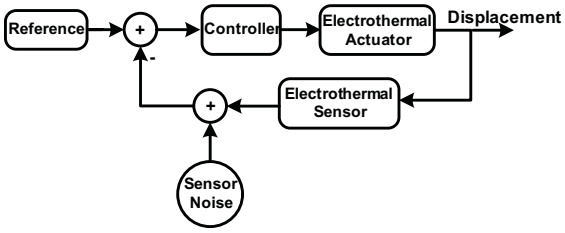

Fig. 1. Micro-actuator feedback loop block diagram.

Among the different sensing and actuation schemes in MEMS, electro-static (capacitive) and electrothermal (resistive) methods have attracted much attention [7]. Capacitive sensing is widely used for displacement measurement in MEMS transducers. One of the issues with this method of sensing is the relatively large footprint of the resulting sensor. Electrothermal sensing has been proposed as an alternative solution [8]. These sensors can be designed to be of a very small form factor, freeing up space that, otherwise, can be used for other purposes, e.g. actuation.

The sensor precision and performance depend on the readout circuitry designed for its output measurement as well as its proper mechanical structure. Regarding the readout circuitry, conventional amplifiers may not be the best option for use as a sensor front-end since their input noise is rather high. Common low frequency signal measurement techniques include low noise amplifiers, auto-zeroing, and chopper modulation [9]. The latter has emerged as a popular sensing front-end for capacitive MEMS transducers since it avoids the $1/f$ noise associated with operational amplifiers by using an amplitude modulation technique. The principle of chopper modulation is to up-convert the signal to higher frequencies where amplifier flicker noise is less than the thermal noise floor. Then, the up-converted signal is amplified and finally down-converted to obtain the original low-frequency signal. The clock feed-through and jitter are the main drawbacks of this method. Chopper amplifier has been proposed for electrothermal sensing in [10]. However, only simulation results are presented and most of the practical issues are ignored.

Manuscript received February 16, 2012; accepted April 19, 2012. Date of publication May 24, 2012; date of current version June 13, 2012. This work was supported in part by Australian Research Council. The associate editor coordinating the review of this paper and approving it for publication was Prof. Sandro Carrara.

A. Mohammadi and S. O. R. Moheimani are with the School of Electrical Engineering and Computer Science, University of Newcastle, Newcastle 2308, Australia (e-mail: mohamadi@ieee.org; reza.moheimani@newcastle.edu.au).

M. R. Yuce is with the Electrical and Computer Systems Engineering, Monash University, Clayton 3800, Australia (e-mail: mehmet.yuce@monash.edu).

Color versions of one or more of the figures in this paper are available online at http://ieeexplore.ieee.org.

Digital Object Identifier 10.1109/JSEN.2012.2198807

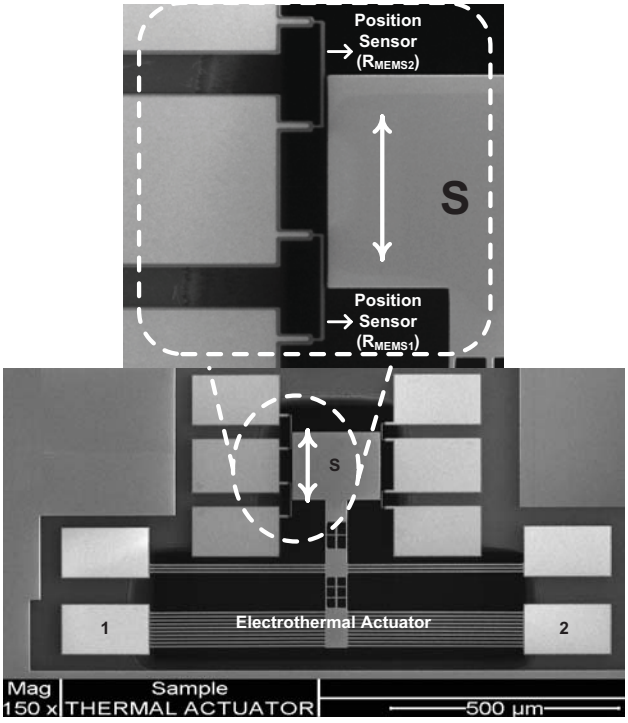

Fig. 2. MEMS-based thermal sensor and thermal actuator.

This work utilizes a frequency modulation (FM) technique to realize a sensor readout circuit for electrothermal sensors. With this method, the signal obtained from the sensor is measured in the frequency domain rather than the amplitude domain. The frequency modulated signals are less prone to amplitude noise. Typicaldistortions on the signal,arising from the electronic circuits, will not normally affect the performance of a FM signal as they are based on frequency, not amplitude. The proposed method features a linear input-output relationship, by combining the nonlinear frequency modulation with inherent nonlinearity of the actuator.

The remainder of the paper continues as follows. In Section II, we have addressed the operation principles of the micro-actuator. In Section III, we propose the frequency based front end for electrothermal sensing including the circuit and the system. Implementation details and experimental results are presented in Section IV which is followed by conclusions.

II. Electrothermal Microactuators

Electrothermal displacement sensors and actuators are commonly fabricated from doped silicon and/or poly-silicon. Fig. 2 shows a one degree of freedom (DOF) MEMS nanopositioner, designed by our group, that works based on the concepts of electrothermal actuation and electrothermal sensing [11]. An input voltage is applied to the actuator component of the device via ports 1, 2. This results in a proportional current passing through the silicon beams of the electrothermal actuator. The actuator' send point is attached to a stage (S), whose movements are to be controlled. The stage functions as a heat absorbing mass, which moves relative to a pair of resistive position sensors (R_{MEMS1}, R_{MEMS2}). The resistance of each sensor is proportional to its temperature. The heat

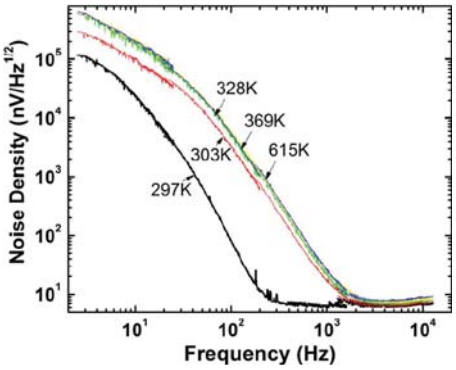

Fig. 3. Doped silicon cantilever noise power density [13].

generated by the resistors is transferred to the mass, which is at a much cooler temperature. The structure of the MEMS device is designed such that the movement of the heat absorber in either direction (up or down in Fig. 2) has opposite effects on the heat transfer rate from the two sensors. Therefore, any displacement would cause a differential variation in the resistances R_{MEMS1} and R_{MEMS2}.

The piezoresistivity of the doped silicon should also be considered for sensors. According to this property the resistance of doped silicon is a function of applied force/stress [7]. Since the beams which are used as the electrothermal sensors in this work are anchored at both sides, the temperature variation results in expansion or contraction. This leads to the stress induced resistivity. In addition to the crystal orientation of silicon, piezoresistivity is a function of doping concentration, type of dopant and the temperature of substrate. Piezoresistivity can be ignored in this application providing that:

1) The parameters that contribute to piezoresistivity affect the sensors in the same way. The differential design of the sensor cancels out their contributions.
2) According to [7], [12], [13], the temperature increase reduces the piezoresistivity of the doped silicon. A typical commercial piezoresistive sensor has a thermal resistance change ten times the full-scale stressed resistance change over a temperature range of 55 °C [12]. The sensors used in this work are heated upto 400–600 °C to increase the thermal sensitivity. Thus their piezoresistivity is substantially reduced.

Furthermore MEMS performance suffers from noise of three distinct sources: mechanical, electrical and quantization noise. Mechanical noise is the thermal agitation of fluid molecules around the proof mass and is also a function of mechanical properties of the device. It is dominant in the surface micromachined devices; however, it's ignorable in the bulk micromachined devices, which provides more flexibility in mechanical properties [14]. Also the system under investigation here is a pure analog one, so the quantizatioin noise doesn't affect the system performance.

Electrical noise is mainly divided into two categories the thermal and the flicker noise. Doped silicon resistors suffer from the flicker noise as well as thermal noise [15]–[17]. Commonly, the flicker noise power overwhelms the thermal noise at low frequencies, as illustrated in Fig. 3. The noise power depends on frequency, the applied current, and the

dimensions of the resistor. According to [15] noise power is proportional to the square of the applied current and inversely proportional to applied signal frequency and cross-sectional area of the resistor. In particular, sensing resistors should be heated up in order to reach adequate sensitivity. A significant current in the order of mA must pass through the resistor to heat it up. Thus, the low frequency noise associated with the resistor becomes significant. More detailed noise formulation is presented in the Appendix.

The electrothermal resistance changes should be measured by the interface circuit. Most readout circuits, proposed in the literature, utilize low noise instrumentation amplifiers. [11], [9]. In addition to the intrinsic flicker (i.e. $1/f$), and thermal noise of the electrothermal sensors, the amplifier noise also adds to the output noise, and thus will degrade the SNR performance of the system. Consequently a higher frequency measurement is likely to reduce the amplifier noise effect on the final result.

The relationship between the applied input voltage and the achieved displacement in a typical MEMS electrothermal actuator is nonlinear. The measurement results for the MEMS actuator in [18] illustrates a quadratic transfer function from the actuation input voltage to displacement. In case of using the available readout circuitries which offer a linear transfer characteristic, the feedback network should compensate the nonlinearity which increases the system complexity. The readout technique proposed here leads to a linear input-output relationship in addition to the sensing at high frequencies to reduce the effect of noise sources.

III. Frequency Modulation Sensing Technique

This section first describes the proposed approach for sensing the resistivity changes corresponding to the electrothermal sensors in the system level. Then, the circuit design procedure including the ring oscillator and front-end circuitry are discussed.

A. Frequency-Based Measurement

Significant efforts have been reported in the literature to develop frequency based measurement methods for resistive sensing [19], [22]. The nonlinear relationship between the input voltage and the output frequency is a common issue with these works. An electrothermal sensor measurement with a high frequency output is reported in [22]. Also an oscillator based signal conditioning is introduced in [19]. Neither of these approaches returns the information in voltage amplitude form, as is needed in a feedback-controlled system. The time based measurement method, introduced in [21] and [20], that is designed for gas sensors, converts large resistance variations in the range of 1 kΩ to 1 GΩ to a measured signal. However, this method is not applicable to MEMS resistive sensors that typically undergo much smaller changes, e.g. less than 10 Ω resistance change here in a 400 Ω sensor.

In this work, a frequency-based measurement is used to avoid the noise contribution of the existing amplifiers to the electrothermal MEMS sensors. Additionally, the circuit configuration is designed to provide a linear relationship between

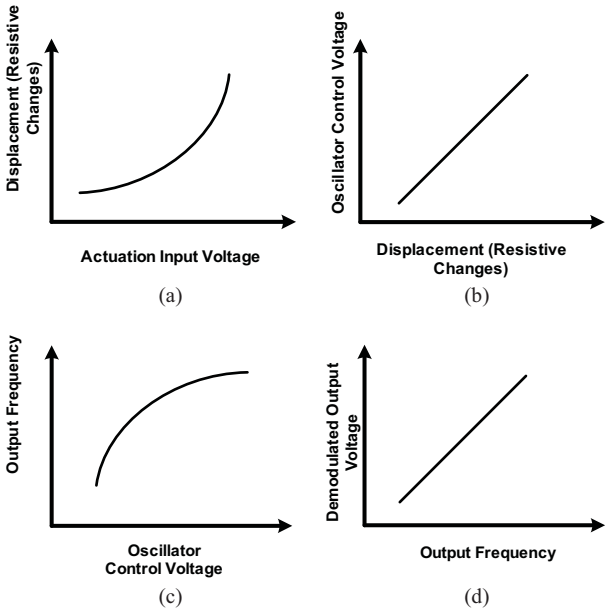

Fig. 4. Proposed method mitigates the nonlinearity from actuation input to the sensor output. (a) Quadratic transfer function (TF) from actuation input to resistive changes. (b) Linear TF from resistive changes to oscillator control voltage. (c) Nonlinear voltage controlled oscillator (VCO) TF from voltage input to frequency output. (d) Linear frequency demodulation.

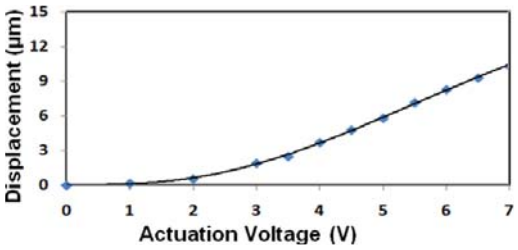

Fig. 5. Nonlinearity of actuator transfer function.

the actuator input and the sensor output voltages. The electrothermal resistive changes, which contain the displacement information associated with the stage (See Fig. 2), demonstrate a nonlinear behavior as shown in Fig. 4(a). The front-end circuit translates the resistive changes to voltage values in a linear way (Fig. 4(b)). Then, the voltage changes result in the frequency variations in a ring oscillator configuration which is inherently nonlinear (Fig. 4(c)). The voltage-frequency characteristic of ring oscillators designed to be inverse of the former nonlinearity. The final output is either a dc, or a slowly varying voltage, which indicates the resistance of the sensor. This voltage is obtained by demodulating the frequency modulated signal (Fig. 4(d)). The measured nonlinearity of transfer function is depicted in Fig. 5. In addition the displacement to resistive changes transfer function adds to this no linearity in the same manner. This has been proved through thermodynamic and electrical analysis. The proposed system's functionality is depicted in Fig. 6. The changes in the sensing resistor translate to frequency variations (F_{IN}) that could be demodulated to a voltage (Fig. 6(a)). As shown, in more details, in Fig. 6(b), electrothermal resistive changes modulate the output frequency of the oscillator VCO1 (voltage controlled oscillator). That is, the output frequency of VCO1 is modulated by changes in the resistance of the electrothermal

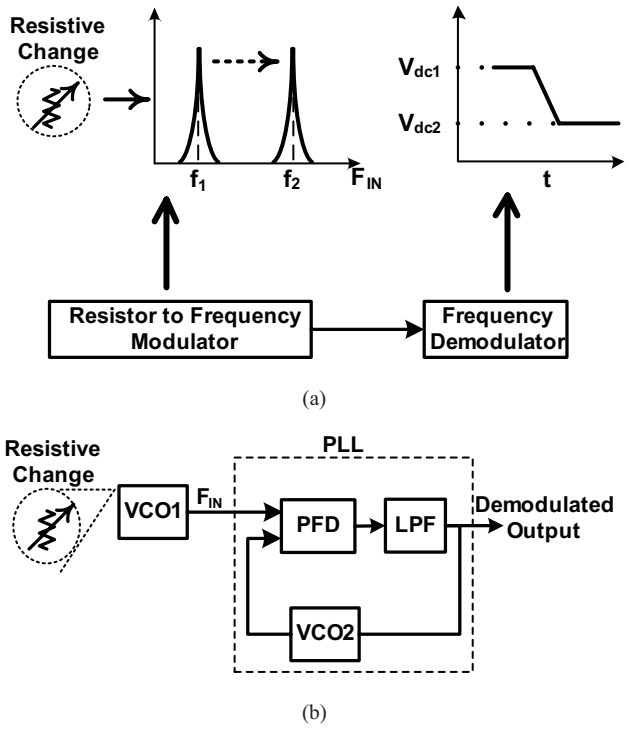

Fig. 6. Proposed frequency based system. (a) System architecture. (b) Frequency demodulation based on PLL.

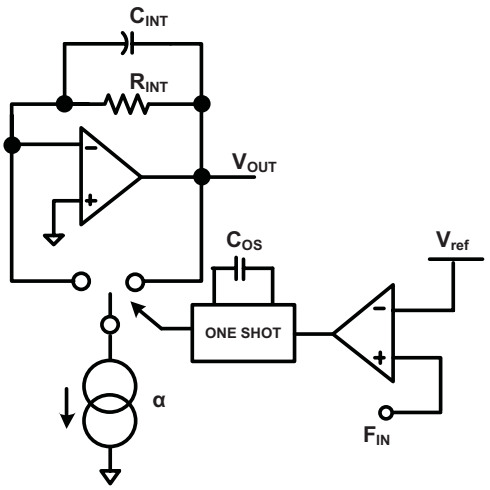

Fig. 7. Alternative frequency demodulation approach.

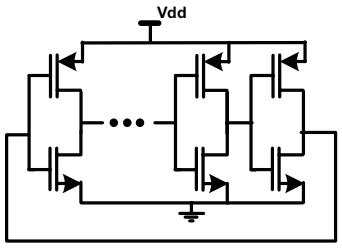

Fig. 8. Ring oscillator using digital inverter chain.

sensor. In order to demodulate the FM signal back to a DC voltage (i.e. sensing voltage).

In the first design, the frequency variations are detected using a phase locked loop (PLL) circuit, which is a widely used frequency demodulation technique. In Fig. 6(b) the output frequency of the reference oscillator (VCO1) is the PLL input frequency (F_{IN}). The phase-frequency detector (PFD) in the PLL compares the two inputs and locks the VCO2's output frequency to the PLL input frequency (F_{IN}). Consequently, the loop follows the VCO1's frequency variations. Until the loop stays in the lock condition, very slight frequency variations appear as phase difference between PFD inputs. The phase difference is extracted by the PFD and transformed to a slowly varying (dc) voltage through a low pass filter (LPF) at the VCO2 input. The frequency-demodulated signal is obtained at the LPF output. PLL FM demodulators have superior linear performance in comparison with the other types of demodulators. While the LPF determines the bandwidth of the demodulated output, it can be utilized to control the low frequency noise. In telecommunication applications where PLLs are used as frequency demodulators, the signal bandwidth is often much wider than what is pursued in this work.

Another popular demodulation approach circuit for frequency modulated signals is frequency to voltage conversion. As illustrated in Fig. 7 the input frequency (F_{IN}) triggers the one-shot circuit which subsequently steers a constant current source (α) to either the output or the summing node of the integrator. This produces a dc voltage proportional to the ON time of the one-shot circuit and the input frequency that is the duty cycle of the current pulse applied to integrator input. Therefore, the current signal at the integrator input will be a pulse wave with a frequency equivalent to F_{IN} and on-time equal to the one-shot time constant (t_{OS}). The integrated output voltage is as follows:

$$V_{OUT} = t_{os}\alpha R_{INT} F_{IN}. \tag{1}$$

A comparison of the two aforementioned frequency demodulation schemes is provided later in section IV.

B. Ring Oscillator

A ring oscillator circuit is utilised to translate the resistive changes to frequency variations as VCO1 in Fig. 6(a). A ring oscillator can be implemented with an odd number of single ended inverters connected in a positive feedback configuration as illustrated in Fig. 8. The oscillation frequency of the system is determined as follows [23]:

$$f_{osc} = \frac{1}{2n\pi\tau}, \quad \tau = RC = \frac{c}{gm}$$
$$f_{osc} = \frac{c}{gm} \tag{2}$$

where, n is the number of stages, and τ is the delay generated by each inverter stage. R represents the inverse of transistor's transconductance (g_m) and C represents the node's capacitance, both of which are varying by the supply voltage. Oscillation frequency can be tuned by manipulating the number of stages, loading, drive strength and supply voltage of inverters. Furthermore, a proper combination of the mentioned methods can result in a wider tuning range [24]. However, changing the supply voltage is the most convenient, and the only practical approach available to us. It also leads to a conveniently wide tuning range. The only disadvantage associated with

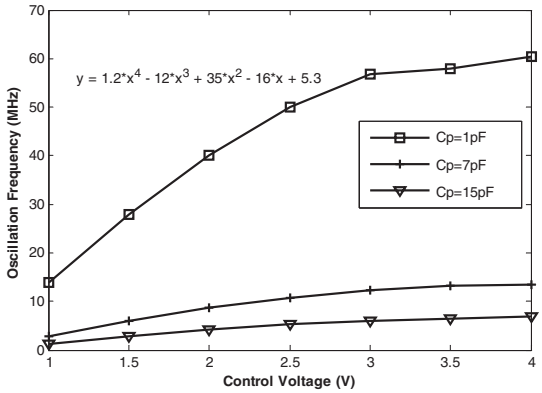

Fig. 9. Simulation of ring oscillator frequency versus supply voltage transfer characteristics.

this method is the presence of a higher level of jitter at low frequencies. Supply induced jitter reduction techniques are discussed in the next section. External large capacitors are added to the inverter input/output nodes to cancel out the voltage variable parasitic capacitances associated with the inverter transistors. Hence, the only viable option to control the oscillation frequency of the system is to manipulate the g_m. A transistor's transconductance is not a linear function of the supplied voltage. This leads to a nonlinear relationship between the supplied voltage and oscillation frequency. The non-linearity of voltage to frequency transfer characteristic of a VCO with differential inverters is explained in [25]. The input control voltage drives the inverter transistors in cut-off, saturation and linear regions. The analytical relationships for all of the operation regions are derived; however the final transfer function is achieved through simulation.

An inverter based ring oscillator has been simulated here. This is established by simulating the operation of a 3-stage inverter-based ring oscillator, consisting of TSMC 0.18 μm CMOS transistors. Simulations were performed on a Spice simulator and the results are illustrated in Fig. 9.

The linearity of the voltage to frequency (V/F) conversion of ring oscillators is a matter of concern in conventional applications, and several linearization techniques have been proposed in the literature, e.g. see. [26], [27]. In the following we illustrate how this inherent nonlinearity can be utilized to mitigate the nonlinear response of electrothermal actuators.

As mentioned before displacement of an electrothermally actuated nanopositioner is a nonlinear function of the actuating voltage [11], [18]. Such quadratic nonlinearities are commonly observed in MEMS electrothermal actuators of various types, as well as in MEMS capacitive actuators. This nonlinearity is very similar to the inverse of the V/F characteristic of a VCO. Thus, by combining the two, one may expect to obtain a relatively linear relationship between the actuating voltage and the measured displacement.This is achivable by selecting a proper value for the node capacitance of the ring oscillator.As illustrated in Fig. 9 the different nonlinear relationships is achievable by using different parasitic capacitors (Cp) at the inverters output node. The curves in Fig. 9 are obtained by simulating the same ring oscillator with different node capacitances. The mathematic

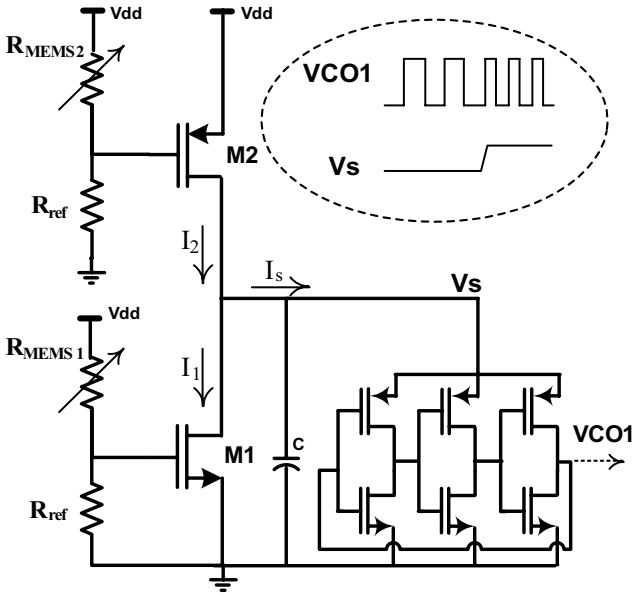

Fig. 10. Circuit designed for VCO1 in proposed system.

relationship is fitted to the curves in MATLAB computer program. For Cp = 1 pF the added parasitic is in the order of parasitic capacitances of transistors. Therefore,the voltage (supply voltage in this case) controls the oscillation frequency through both transcondactance and internal capacitances of the transistors. However for Cp = 7, 15 pF the added capacitance dominates the node capacitance value so the denominator of (2) is fixed with respect to control voltage. Accordingly in the experiments we use large capacitances to control the achivable nonlinearity.

Electronic oscillators used in telecommunication systems generally suffer from phase noise. Phase noise in the frequency domain translates to jitter in the time domain. The phase noise phenomenon in ring oscillators has been discussed in [28]. The main contributor to the phase noise close to the center frequency is the flicker noise of the inverters' tail current supply that up-converts into the close vicinity of the oscillation frequency. Insertion of a large capacitor between the supplying tail current and the ground, as illustrated in Fig. 10, can be used to reduce this noise [29]. The large capacitance, when combined with the output impedance of the current source acts like a low-pass filter and suppresses the flicker noise at the baseband, avoiding its up-conversion.

We have utilized the available simple digital gates at the inverter chain to explain the operation of ring oscillators. However, digital gate inverters cause degradations in phase noise performance of ring oscillators in comparison with the differential and current steering inverters [30]. Further improvement can be achieved by replacing voltage supplies with current sources. This has been shown to lead to 4 to 6 dB phase noise reduction at the same oscillation frequency with similar design parameters [31].

C. Front-End Circuit Design

In order to convey the resistive changes to oscillator control voltage the simple interface circuit including M1, M2 and reference resistors is designed as shown in Fig 10. Since M1

and M2 are designed to operate in saturation the input-output transfer characteristic is supposed to be linear.

Applying the aforementioned phase noise reduction techniques, a ring oscillator circuit with better noise properties was designed. The circuit depicted in Fig. 10, is designed to replace the reference oscillator VCO1 in Fig. 6(b). This circuit transforms the variations in the electrothermal sensor's resistance to frequency variations. As a result, the oscillation frequency of ring oscillator is a function of the MEMS resistor and consequently the actuator displacement. The reference resistor (R_{ref}) is a discrete (lumped) resistor selected to be almost the same value as the MEMS electrothermal sensor resistance. This is clarified through the following explanation.

Assuming $R_{MEMS} = x$ and $R_{ref} = y$, the M1 gate voltage is as follows:

$$V_g(x, y) = V_{dd}\frac{y}{x+y}. \tag{3}$$

The sensitivity of Vg to x is therefore defined as in (4)

$$S_x^{V_g} = \frac{\partial V_g}{\partial x} = V_{dd}\frac{-y}{(x+y)^2}. \tag{4}$$

In order to maximize the sensitivity of the circuit to MEMS electrothermal resistor changes, the maximum of S_x with respect to y should be found. Differential equation (5) is obtained by taking the partial derivative of (4) with respect to y

$$\frac{\partial S_x^{V_g}}{\partial y}\frac{\partial^2 V_g}{\partial y \partial x} = V_{dd}\frac{y-x}{(x+y)^3} \tag{5}$$

$$\frac{\partial S_x^{V_g}}{\partial y} = 0 \rightarrow x = y. \tag{6}$$

From (6) it is inferred that the maximum sensitivity of the circuit to R_{MEMS} variations will be achieved if $R_{ref} = R_{MEMS}$. Fortunately, this coincides with the optimum bias point of M1 to operate in saturation mode.

The power supply induced jitter requires attention since the noise from the MEMS devices reaches the supply line of the ring oscillator by going through M1 and M2. This noise, as indicated earlier, has a low pass characteristic. According to [30], a digital gate has a low-pass transfer function from the power supply to output of the ring oscillator, while the differential pair and the current steering gates have a high-pass nature. Obviously, we may expect better noise performance for the system if the high-pass transfer functions of those inverters filter out the supply induced noise.

Here, the oscillator was realized from off-the-shelf digital gates. This is expected to affect the overall noise performance of the proposed scheme since they pass the supply noise, which is affected by the noise of MEMS devices. Thus, in order to suppress the noise over the lowest possible frequency ranges, a large noise canceling capacitance (C in Fig. 10) is connected to the common drain of M1, and M2, both of which are operating as tail current sources. Each of these techniques significantly improves the implemented circuit performance in terms of phase noise and jitter.

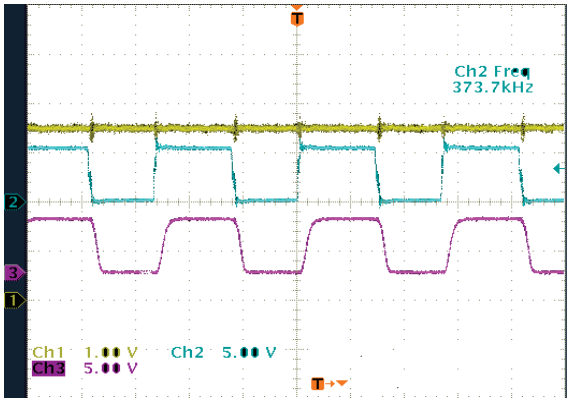

Fig. 11. Tracking VCO outputs and FM demodulated output: Ch2 (VCO1 output), Ch3 (VCO2 output), and Ch1 (demodulated output).

IV. Experiments and Discussion

The sensing technique explained in Section III has been applied to the MEMS nanopositioner reported in [11]. The device is utilized as an electrothermal displacement sensor. Electrothermal position sensor resistors, (R_{MEMS1}, R_{MEMS2} in Fig. 2, Fig. 10) are connected in series with the reference resistors of the same values to a 5 v dc supply (V_{dd} in Fig. 10). The actuation mechanism of this device is also electrothermal. By applying the variable actuation voltage (0∼5 V) to ports 1, 2 in Fig. 2, the stage (which functions as the heat absorber for electrothermal sensors) moves relative to the hot sensor resistors. Since the stage is cooler than the sensors, it absorbs the heat and changes the sensor resistance. The sensing circuit is implemented using off-the-shelf integrated circuits (ICs) as follows. M1 and M2 in Fig. 10 are implemented using CD4007 [32], which contains three NMOS and three PMOS transistors. In order to adjust the quiescent points of M1 and M2 (as it was impossible to change the aspect ratio of the transistors) two NMOS and three PMOS transistors were connected in parallel. The ring oscillator is realized from five 74HC04 inverters [33]. First a PLL based demodulation technique used to recover the sensing signals. Phase/frequency detector (PFD) and VCO2 of Fig. 6(b) are integrated in 74HC4046, which is a PLL IC. [34]. The low pass filter is externally connected to the PLL.

As illustrated in Fig. 11 the experimental results show that VCO1 and VCO2 track each other while the PLL is in phase lock condition. The demodulated output is represented with Ch1. Oscillation frequency of VCO1 increases from 390 kHz to 550 kHz for the actuation input voltage varying from 1 v to 6 v. The dc demodulated output varies almost linearly from 3.4 V to 4.8 V for the same actuation voltages as shown in Fig. 11. Therefore the output voltage which is going to be used as a feedback signal is a linear function of input actuation voltage. This could be comparable the previous work in which a look-up table was designed in feedback path to mitigate the nonlinearity of forward path [11].

As indicated in Section III, the linearity of the transfer function from the input actuation voltage to the last sensor output in micro-actuators is highly desirable. A ring oscillator generates a nonlinear transfer function from the input voltage

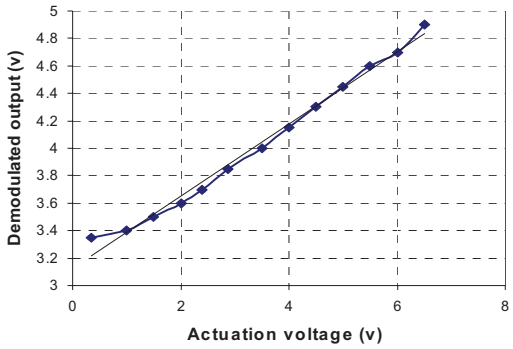

Fig. 12. Demodulated output versus actuation voltage.

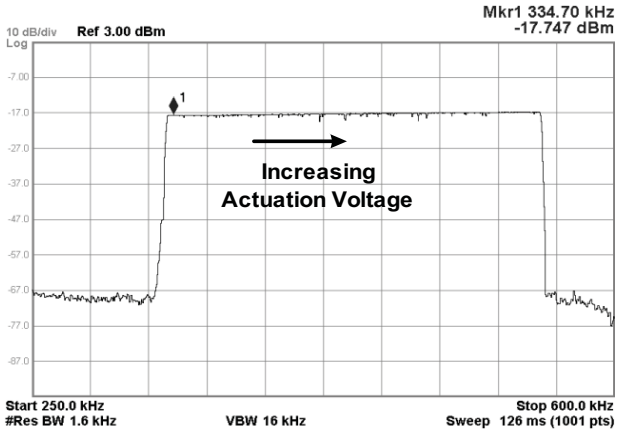

Fig. 13. Ring oscillator frequency versus actuation voltage.

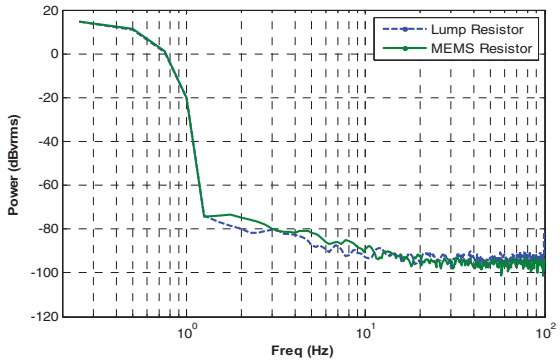

Fig. 14. Noise power spectrum of demodulated output.

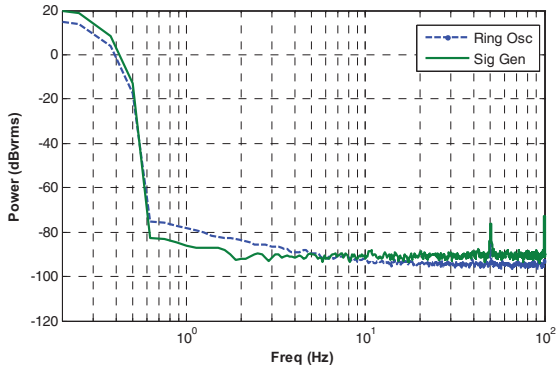

Fig. 15. Noise power spectrum of frequency to voltage converter (AD650).

to the output frequency. By placing the ring oscillator after the front-end of the readout circuitry we managed to achieve an almost linear relationship between the signal applied to the actuator (which is a nonlinear device) and the last sensed voltage, as shown in Fig. 12. Also Fig. 13 is obtained by Agilent spectrum analyzer (N9020A) tracing the output spectrum of the oscillator while the actuation voltage was being increased.

Power spectral density of the measured low frequency signal is shown in Fig. 14. The data was acquired using a HP 35670A dynamic signal analyzer. The low frequency noise is shown at various offset frequencies. In particular, -72 dB vrms output noise power is achieved at 2 Hz offset frequency. In order to demonstrate the MEMS resistor's noise contribution it was replaced with a lumped resistor, of the same resistance. About 10 dB noise power difference can be observable in the 2-20 Hz frequency range. This implies that, in addition to the flicker noise discussed in part II of this paper, the sensing system is prone to thermal noise arising from the heated MEMS resistors. During these experiments the lumped resistor was kept at the room temperature.

The most common approach to frequency demodulation involves using a PLL. However, in order to understand the overall frequency modulation technique clearly, such as the relationship between the actuation voltage and the demodulated output voltage and the noise performance, a frequency to voltage converter circuit is also implemented, shown in Fig. 7, [35]. The ring oscillator output VCO1 was applied to the frequency input of the AD650. The output spectrum is illustrated in Fig. 15. In order to determine contributions of VCO1 and the front-end to the resulting low frequency noise a signal generator was directly applied to the AD650. The result is about 10 dB lower noise power at 1 Hz. The difference is obviously generated by a combination of the MEMS device and the oscillator circuit. The former could be improved by some modifications in the mechanical design of the device, while the latter requires an improvement of the utilized circuit design techniques and components.

Since the two demodulators are implemented with different off-the-shelf devices, a fair comparison of their performances may be rather difficult. However, the second approach requires fewer components and involves a simpler architecture to realize the requisite demodulation circuit. Thus, it has the potential to result in less noise at the output. Furthermore, in the first approach, the input signal bandwidth follows that of the PLL's, which is directly proportional to its lock range. Moreover, due to the trade-off between the PLL bandwidth and the phase noise passed through the PLL, a narrower bandwidth is desired. This constraint does not apply to the second approach. Instead, the settling accuracy of the circuit shown in Fig. 7 is determined by the integrator's R and C. Besides, the dc output voltage generated by F/V converter depends on the power supply and could be wide enough.

A comparison of the proposed system with similar circuits proposed for resistive sensing in the literature is summarized in table 1. They differ in the resistance variation range and its temperature. In the application pursued here, the resistors are

TABLE I
COMPARISON BETWEEN RESISTIVITY SENSORS

Parameters	[10]	[20]	[36]	This paper
Resistor variation	Not reported	1MΩ-1GΩ	4KΩ	400–410Ω
Sensitivity	1000V/V*	Not reported	1V/%1 of resistance variation	2V for 2.5% of resistance variation
Linearity	Linear	Linear	Linear	nonlinear
Implementation	Simulation	Off-the-shelf devices	0.35μm CMOS	Off-the-shelf devices
Application	Thermo-pile	Gas sensor	Strain gauge (Surface micro-machined MEMS)	Electro-thermal displacement sensor (Bulk micro-machined MEMS)
Circuit architecture	Chopper amplifier	Resitivity to period converter	Active wheat-stone bridge	Frequency modulation

*Only the voltage gain is reported.

heated up to increase the sensitivity of device vs. temperature. On the other hand the output noise level increases as a heating consequence. Also the nonlinear circuit designed in this work combines with the nonlinearity of the actuator and produces a linear input-output relationship. However the interface circuits designed in [10], [20], [36] are linear readout front–ends which are not suitable for this application.

V. CONCLUSION

A highly sensitive sensor readout circuit is designed and implemented. The readout circuit uses a frequency modulation and demodulation technique to sense the changes of a MEMS-based electrothermal sensor's resistance. A linear relationship between the input actuation voltage and sensor output signal has been achieved while maintaining the same noise performance as other high sensing measurement techniques. After actuation, the variation in the sensing element is frequency modulated using a ring oscillator, oscillating in the frequency range of 350–550 kHz. Thus, the sensing is done at a much higher frequency than the low frequency ranges where there are noise sources.

A practical demodulation circuit is implemented to recover the modulated sensing signal. Experimental results demonstrate about −72 dB Vrms output noise floor at the 2 Hz offset frequency. Noise contribution due to the doped silicon is also characterized and discussed. Furthermore, the overall transfer characteristic from the input actuation voltage to the sensor output is almost linear. The off-the-shelf components are used to realize a practical system as a proof of concept. However, more competitive results can be expected from an application specific integrated circuit design of the proposed circuit.

APPENDIX

Thermal noise which is generated by electrothermal sensors or micro-heaters is significantly higher than ordinary resistors because of their high temperature. Theoretical thermal (Johnson) noise for resistive devices and flicker noise for almost all electronic components are as following:

$$V_J = (4k_B T R)^{\frac{1}{2}} \left[\frac{V}{H Z^{\frac{1}{2}}} \right] \tag{A-1}$$

where k_B is the Boltzmann constant, R and T are the resistance and temperature of the device, and

$$V_f = \left(K R^2 \left(\frac{I^a}{f^b} \right) \right)^{\frac{1}{2}} \left[\frac{V}{H Z^{\frac{1}{2}}} \right] \tag{A-2}$$

where K is a constant for the device, I is a direct current, f is frequency and a and b are constants.

ACKNOWLEDGMENT

The authors would like to thank Dr. Y. Zhufor the design and fabrication of the microelectromechanical systems (MEMS) device used in this paper, Dr. A. N. Laskovski for his advice on measurement techniques and D. Phelan, School of Medical Sciences, University of Newcastle, Newcastle, Australia, for his help on scanning electron microscope images of MEMS device.

REFERENCES

[1] G. Binning and H. Rohrer, "The scanning tunneling microscope," *Sci. Amer.*, vol. 253, pp. 50–56, Oct. 1986.
[2] G. Binning, C. Quate, and C. Gerber, "Atomic force microscope," *Phys. Rev. Lett.*, vol. 56, no. 9, pp. 930–933, 1986.
[3] N. B. Hubbard, M. L. Culpepper, and L. L. Howell, "Actuators for micropositioners and nanopositioners," *Trans. ASME*, vol. 59, no. 6, pp. 324–334, Nov. 2006.
[4] B. Felix, N. Adrian, O. Stefano, J. B. Dominik, S. Yu, D. Jrg, and J. N. Bradley, "Monolithically fabricated microgripper with integrated force sensor for manipulating microobjects and biological cells aligned in an ultrasonic field," *J. Microelectromech. Syst.*, vol. 16, no. 1, pp. 7–15, 2007.
[5] B. K. Chen, Z. Yong, and S. Yu, "Active release of microobjects using a MEMS microgripper to overcome adhesion forces," *J. Microelectromech. Syst.*, vol. 18, no. 3, pp. 652–659, Jun. 2009.
[6] R. K. Messenger, Q. T. Aten, T. W. Mclain, and L. L. Howell, "Piezoresistive feedback control of a MEMS thermal actuator," *J. Microelectromech. Syst.*, vol. 18, no. 6, pp. 1267–1278, Dec. 2009.
[7] C. Liu, *Foundations of MEMS*, 2nd ed. Upper Saddle River, NJ: Prentice-Hall, 2012.
[8] M. A. Lantz, G. K. Binnig, M. Despont, and U. Drechsler, "A micromechanical thermal displacement sensor with nanometer resolution," *Nanotechnology*, vol. 16, no. 8, pp. 1089–1094, Aug. 2005.
[9] C. C. Enz, E. A. Vittoz, and F. Krummenacher, "A CMOS chopper amplifier," *IEEE J. Solid-State Circuits*, vol. 22, no. 3, pp. 335–342, Jun. 1987.
[10] M. Dei, P. Bruschi, and M. Piotto, "Design of CMOS chopper amplifiers for thermal sensor interfacing," in *Proc. Res. Microelectron. Electron. PRIME Ph.D.*, Jun. 2008, pp. 205–208.
[11] Y. Zhu, A. Bazaei, S. O. R. Moheimani, and M. R. Yuce, "A micromachined nanopositioner with on-chip electrothermal actuation and sensing," *IEEE Electron Device Lett.*, vol. 31, no. 10, pp. 1161–1163, Oct. 2010.
[12] A. A. Barlian, W. T. Park, J. R. Mallon, A. J. Rastegar, and B. L. Pruitt, "Review: Semiconductor piezoresistance for microsystems," *Proc. IEEE*, vol. 97, no. 3, pp. 513–552, Mar. 2009.

[13] J. Liu, M. Noman, J. A. Bain, T. E. Schlesinger, and G. K. Fedder, "Polysilicon sensors for CMOS-MEMS electrothermal probes," in *Proc. Int. Conf. Solid-State Sensors Actuat. Microsyst. TRANSDUCERS*, Jun. 2009, pp. 2425–2428.
[14] V. Kajaakari, *Practical MEMS*. Las Vegas, NV: Small Gear Publication, 2009, pp. 41–45.
[15] E. A. Corbin and W. P. King, "Electrical noise characteristics of a doped silicon microcantilever heater-thermometer," in *Proc. IEEE Sensors*, Nov. 2010, pp. 2373–2376.
[16] R. Brederlow, W. Weber, C. Dahl, D. Schmitt-Landsiedel, and R. Thewes, "Low-frequency noise of integrated polysilicon resistors," *IEEE Trans. Electron Devices*, vol. 48, no. 6, pp. 1180–1187, Jun. 2001.
[17] P. Srinivasan, W. Xiong, and S. Zhao, "Low-frequency noise in integrated N-WELL resistors," *IEEE Electron Device Lett.*, vol. 31, no. 12, pp. 1476–1478, Dec. 2010.
[18] A. Jungen, C. Meder, M. Tonteling, C. Stampfer, R. Linderman, and C. Hierold, "A MEMS actuator for integrated carbon nanotube strain sensing," in *Proc. IEEE Sensors*, Oct.–Nov. 2005, pp. 93–96.
[19] V. Ferrari, C. Ghidini, D. Marioli, and A. Taroni, "Oscillator-based signal conditioning with improved linearity for resistive sensors," *IEEE Trans. Instrum. Meas.*, vol. 47, no. 1, pp. 293–298, Feb. 1998.
[20] A. Flammini, D. Marioli, and A. Taroni, "A low-cost interface to high-value resistive sensors varying over a wide range," *IEEE Trans. Instrum. Meas.*, vol. 53, no. 4, pp. 1052–1056, Aug. 2004.
[21] M. Grassi, P. Malcovati, and A. Baschirotto, "A 141-dB dynamic range CMOS gas-sensor interface circuit without calibration with 16-bit digital output word," *IEEE J. Solid-State Circuits*, vol. 42, no. 7, pp. 1543–1554, Jul. 2007.
[22] S. H. Tseng, C. L. Fang, P. C. Wu, Y. Z. Yuang, and M. S. C. Lu, "A CMOS MEMS thermal sensor with high frequency output," in *Proc. IEEE Sensors Conf.*, Oct. 2008, pp. 387–390.
[23] J. A. Mcneill and D. S. Ricketts. (2009). *The Designer's Guide to Jitter in Ring Oscillators* [Online]. Available: http://www.springer.com/engineering/circuits+%26+systems/
[24] X. Zhao, R. Chebli, and M. Sawan, "A wide tuning range voltage-controlled ring oscillator dedicated to ultrasound transmitter," in *Proc. 16th Int. Conf. Microelectron.*, Dec. 2004, pp. 313–316.
[25] C. Huiting and R. Geiger, "Transfer characterization of CMOS ring voltage controlled oscillators," in *Proc. 44th IEEE Midwest Symp. Circuits Syst.*, Aug. 2001, pp. 66–70.
[26] L. Changzhi and L. Jenshan, "A 1–9 GHz linear-wide-tuning-range quadrature ring oscillator in 130 nm CMOS for non-contact vital sign radar application," *IEEE Microw. Wireless Compon. Lett.*, vol. 20, no. 1, pp. 34–36, Jan. 2010.
[27] C. Jaehyouk, L. Kyutae, and J. Laskar, "A ring VCO with wide and linear tuning characteristics for a cognitive radio system," in *Proc. IEEE Radio Freq. Integr. Circuits Symp.*, Apr. 2008, pp. 395–398.
[28] A. A. Abidi, "Phase noise and jitter in CMOS ring oscillators," *IEEE J. Solid-State Circuits*, vol. 41, no. 8, pp. 1803–1816, Aug. 2006.
[29] L. Dai and R. Harjani, "Analysis and design of low-phase-noise ring oscillators," in *Proc. Int. Symp. Low Power Electron. Design*, 2000, pp. 289–294.
[30] T. Pialis and K. Phang, "Analysis of timing jitter in ring oscillators due to power supply noise," in *Proc. Int. Symp. Circuits Syst.*, May 2003, pp. 685–688.
[31] M. Grozing and M. Berroth, "Reduction of CMOS inverter ring oscillator close-in phase noise by current mode instead of voltage mode supply," in *Proc. Res. Microelectron. Electron. PRIME Ph.D.*, 2006, pp. 97–100.
[32] Texas Instruments, Inc. (2003). *MOS Package Datasheet*, Dallas, TX [Online]. Available: http://www.focus.ti.com
[33] NXP. (1993). *Digital Inverter Datasheet*, Lake Forest, CA [Online]. Available: http://www.nxp.com
[34] NXP. (1997). *Phase Locked Loop Data Sheet*, Lake Forest, CA [Online]. Available: http://www.nxp.com
[35] S. Martin, "Using the AD650 voltage-to-frequency converter as a frequency-to-voltage converter," Analog Devices, Norwood, MA, Tech. Rep. AN-279, 2009.
[36] E. M. Boujamaa, B. Alandry, S. Hacine, L. Latorre, F. Mailly, and P. Nouet, "A low power interface circuit for resistive sensors with digital offset compensation," in *Proc. IEEE Int. Symp. Circuits Syst.*, May–Jun. 2010, pp. 3092–3095.

Ali Mohammadi (S'09) received the B.Sc. and M.Sc. degrees in electrical and electronics engineering from Urmia University, Urmia, Iran, and the Iran University of Science and Technology, Tehran, Iran, in 2003 and 2007, respectively. He is currently pursuing the Ph.D. degree from the University of Newcastle, Newcastle, Australia.

His current research interests include mixed mode integrated circuit design with specific focus on interface circuits for microelectromechanical systems devices.

Mehmet Rasit Yuce (S'01–M'05–SM'10) received the M.S. degree in electrical and computer engineering from the University of Florida, Gainesville, in 2001, and the Ph.D. degree in electrical and computer engineering from North Carolina State University (NCSU), Raleigh, in 2004.

He joined the Department of Electrical and Computer Systems Engineering, Monash University, Clayton, Australia, in July 2011. He was a Research Assistant with the Department of Electrical and Computer Engineering, NCSU, from August 2001 to October 2004. He was a Post-Doctoral Researcher with the Electrical Engineering Department, University of California, Santa Cruz, in 2005. He was a Senior Lecturer with the School of Electrical Engineering and Computer Science, University of Newcastle, Newcastle, Australia, until July 2011. He has published more than 80 technical articles in the above areas. He is an author of the book *Wireless Body Area Networks* in 2011. His current research interests include wireless implantable telemetry, wireless body area network, bio-sensors, microelectromechanical systems sensors, integrated circuit technology dealing with digital, analog, and radio frequency (RF) circuit designs for wireless, biomedical, and RF applications.

Dr. Yuce received the NASA Group Achievement Award in 2007 for developing silicon on insulator transceiver and the Research Excellence Award from the Faculty of Engineering and Built Environment, University of Newcastle, in 2010. He is a member of the professional societies, the IEEE Solid-State Circuit Society, the IEEE Engineering in Medicine and Biology Society, and the IEEE Circuits and Systems Society.

S. O. Reza Moheimani (F'11) received the Ph.D. degree in electrical engineering from Australian Defence Force Academy, University of New South Wales, Canberra, Australia, in 1996.

He joined the University of Newcastle, Newcastle, Australia, in 1997, where he founded and directs the Laboratory for Dynamics and Control of Nanosystems, a multimillion-dollar state-of-the-art research facility. He is a Professor and an Australian Research Council Future Fellow with the School of Electrical Engineering and Computer Science, University of Newcastle. He has held several visiting appointments with IBM Zurich Research Laboratory, Zurich, Switzerland. His current research interests include dynamics and control at the nanometer scale and include applications of control and estimation in nanopositioning systems for high-speed scanning probe microscopy, modeling and control of microcantilever-based devices, control of electrostatic microactuators in microelectromechanical systems, and control issues related to ultrahigh-density probe-based data storage systems.

Prof. Moheimani is a fellow of the International Federation of Automatic Control and the Institute of Physics, U.K. He was a co-recipient of the IEEE TRANSACTIONS ON CONTROL SYSTEMS TECHNOLOGY Outstanding Paper Award in 2007 and the IEEE Control Systems Society Control Systems Technology Award in 2009, the latter together with a group of researchers from the IBM Zurich Research Laboratory. He has served on the editorial boards of a number of journals, including the IEEE TRANSACTIONS ON CONTROL SYSTEMS TECHNOLOGY, the IEEE/American Society of Mechanical Engineers TRANSACTIONS ON MECHATRONICS, and *Control Engineering Practice*, and has chaired several international conferences and workshops.